Next Generation Tunable Microwave Cavities for the search of Dark Matter Axions using Nonlinear Dielectric Films

Summer Internship in Science and Technology

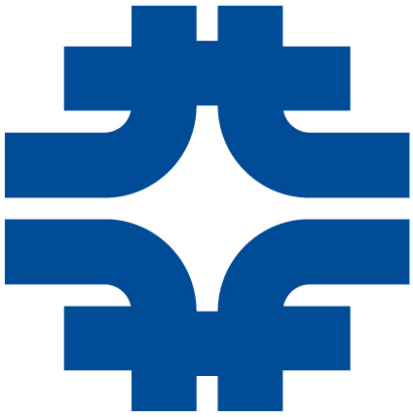

Marlene Ortega
Department of Physics
Brown University

Supervisor: Daniel Bowring
With support from Aaron Chou, Andrew Sonnenschein, and Alvin Tollestrup
Fermi National Accelerator Laboratory
August 17, 2017

Next Generation Tunable Microwave Cavities for the search of Dark Matter Axions using Nonlinear Dielectric Films

Marlene Ortega

Brown University

Daniel Bowring

Fermi National Accelerator Laboratory

(Axion Dark Matter eXperiment)

(Dated: August 17, 2017)

Abstract

The axion is one of the most well-motivated dark matter candidates. Arising from the Peccei-Quinn solution to the strong CP problem, it has the potential to be one of the lightest elementary particles, on the order of 10^6 to 10^3, as well as one of the most weakly interacting. Experiments such as the Axion Dark Matter eXperiment (ADMX) use high-Q, tunable microwave cavities permeated by a strong magnetic field to stimulate the axion Primakoff interaction. The tunability of the cavity resonance frequency is crucial, allowing for efficient scanning of the large axion mass range. Future iterations of the ADMX microwave cavity experiment will require methods to finely tune cavities. A promising method for achieving this sensitive frequency response is to coat the walls of the cavity with a nonlinear dielectric material. The resonant frequency of the cavity depends on the dielectric constant as $f \propto \frac{1}{\sqrt{\epsilon_{eff}}}$, while ϵ_{eff} depends on the temperature and voltage applied to the films. Thus, a large shift in the dielectric constant of the cavity would provide a wide range in axion masses. Using a nonlinear dielectric film as an additional fine tuning method would save space inside the magnet, introduce minimal noise and mitigate the thermal noise caused by the tuning rods. In this report, we characterize the behavior of a nonlinear dielectric material, Strontium Titanate $SrTiO^3$ (STO), at low temperatures using a coplanar waveguide resonator. By using an analytic model of system, we isolate the dielectric constant of thin STO films and investigate the feasibility of using STO as a tuning mechanism. We find that while there is a noticeable shift in dielectric constant attributable to STO, further research with pure STO samples is necessary.

I. INTRODUCTION

In 1933, the Swiss-American Astronomer Fritz Zwicky discovered that the velocities of galaxies within the Coma cluster implied that there was a gravitational attraction between them greater than what could be accounted for by the luminous matter. Assessments of orbital speed within individual galaxies done by Vera Rubin, Kent Ford, and Albert Bosma in the 1970s revealed that galaxies had a nearly flat rotation curve: again, orbital velocities at distances far from the galactic center were much faster than what was justified by the amount of baryonic matter, reaffirming Zwickys results. Thus, observational evidence at the galactic scale was consistent with evidence on the scale of galaxy clusters. These two experiments were the observational foundation for dark matter: once accepted by the larger physics community, the techniques that could measure the effects of dark matter in the universe and theories that could explain these effects grew exponentially.

Today, evidence such as the influence of dark matter on the CMB, weak gravitational lensing of distant galaxies, simulations of galactic evolution, and astronomical objects such as the Bullet Cluster proves that dark matter must exist in great quantities. All this evidence strongly indicates that 80 to 85% of the matter in the universe consists of non-luminous and non-baryonic material. The unknown nature of dark matter now poses one of the greatest challenges to modern day physics. An interesting development over the last few years is that the growing intersection between the fields of cosmology, astrophysics and particle physics, has made it so that many theories that solve large problems in the Standard Model of particle physics also explain these observations.

The axion, a theoretical elementary particle arising from the Peccei-Quinn solution to the Strong CP problem, is one of these well-motivated dark matter candidates. It has the potential to be one of the lightest elementary particles, on the order of 10^6 to 10^3, as well as one of the most weakly interacting. Axions appear naturally in string theories, and nonthermal axions produced during the QCD phase transitions become nonrelativistic early enough in the universe so that they were caught in the gravitational wells of galaxies as they formed. Astrophysical and cosmological limits constrain the mass of the axion, 1 to 1000 μeV, and give it the necessary relic density to constitute the majority of matter in the universe.

Experiments such as the Axion Dark Matter eXperiment (ADMX) are currently under-

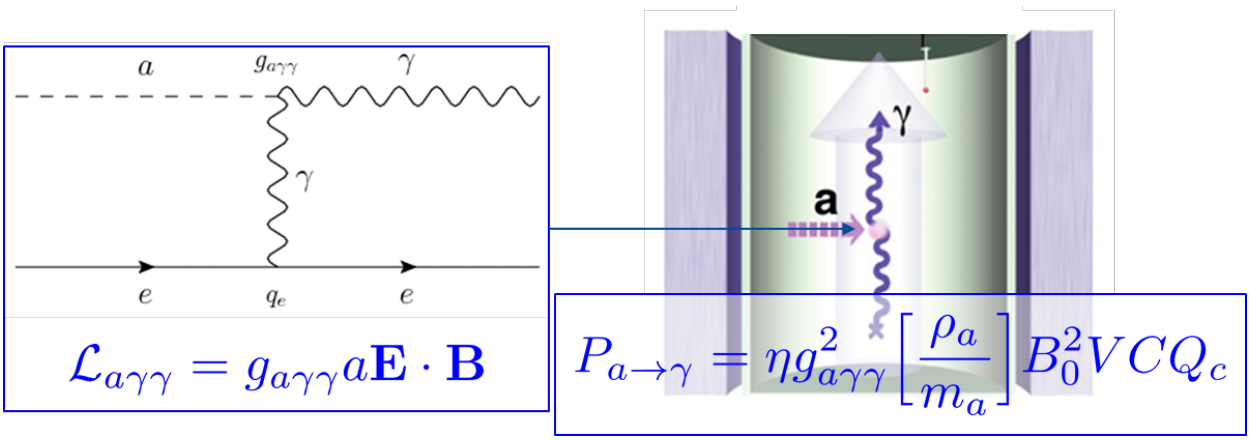

FIG. 1: The Axion Primakoff Interaction. An axion couples to the magnetic field and resonantly converts into a photon. In a microwave cavity, this produces an electric signal with power on the yoctowatt scale.

way to find these particles in the dark matter halo of the Milky Way. ADMX uses high-Q, tunable microwave cavities permeated by a strong magnetic field to stimulate the axion Primakoff interaction. The tunability of the cavity resonance frequency is crucial, allowing for efficient scanning of the large axion mass range. Future iterations of the ADMX microwave cavity experiment will require methods to finely tune cavities. A promising method for achieving this sensitive frequency response is to coat the walls of the cavity with a nonlinear dielectric material. The resonant frequency of the cavity depends on the dielectric constant as $f \propto \frac{1}{\sqrt{\epsilon_{eff}}}$, while ϵ_{eff} depends on the temperature and voltage applied to the films. Thus, a large shift in the dielectric constant of the cavity would provide a wide range in axion masses. Using a nonlinear dielectric film as an additional fine tuning method would save space inside the magnet, introduce minimal noise and mitigate the thermal noise caused by the tuning rods. In this report, we characterize the behavior of a nonlinear dielectric material, Strontium Titanate $SrTiO^3$ (STO), at low temperatures using a coplanar waveguide resonator. By using an analytic model of system, we isolate the contribution to the total capacitance of the thin STO films and isolate the dielectric constant of STO.

II. THE AXION DARK MATTER EXPERIMENT

Experiments such as the Axion Dark Matter eXperiment (ADMX) are designed to detect axions in the dark matter halo of the Milky Way through the Primakoff process. As shown in Fig. 1, the axions resonantly convert into photons within the microwave cavity permeated

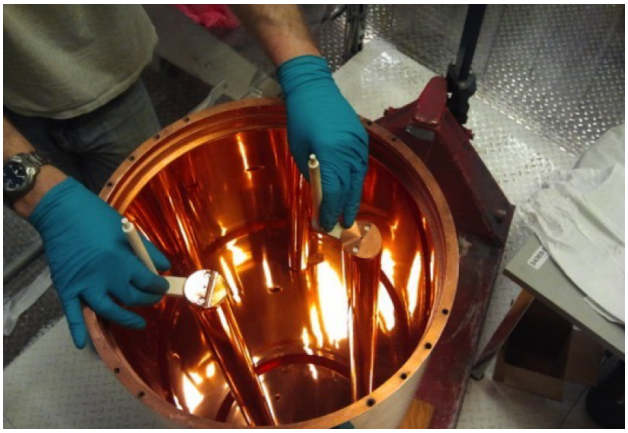

(a) The "Haloscope." ADMX's current tunable cavity used to search for dark matter axions in the halo of the Milky Way [1].

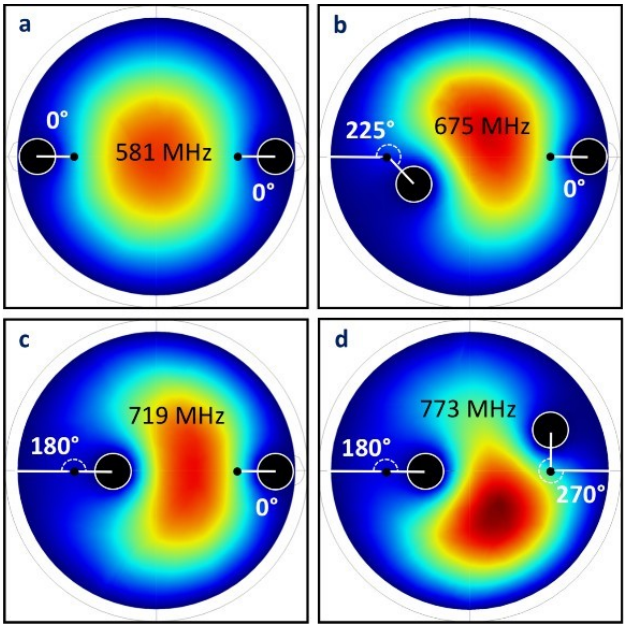

(b) Simulation of the change in frequency as the position of the rods changes [2].

FIG. 2: The current generation of microwave resonant cavities for ADMX, the "Haloscope."

by a strong magnetic field, producing a weak signal.

A. ADMX Generation 1

The ADMX G1 apparatus consists of an 7 T magnet and a cryogenically cooled, high-Q, tunable microwave cavity, or "Haloscope". By slowly adjusting positions of two tuning rods within the cavity, the resonant frequency of the cavity changes, as shown in Fig. 2. The axion-photon conversion results in a signal with power on the yoctowatt (10^{-24} watt) scale, given by Eq. 1.

$$P_{a\to\gamma} = \eta g_{a\gamma\gamma}^2 \left[\frac{\rho_a}{m_a}\right] B_0^2 V C Q_c \tag{1}$$

Where η is the fraction of the converted power which is coupled to a detector, $g_{a\gamma\gamma}$ is the axion-photon coupling constant, ρ_a is the local axion density, m_a is the axion mass, B_0 is the strength of the magnetic field, V is the volume of the cavity, C is a form factor, and Q_c is the quality factor of the cavity.

Such a small signal power necessarily requires noise to be minimized. Using a 3He refrigerator, the apparatus can be cooled down to below 200 mK. Amplification of the signal by Superconducting QUantum Interference Devices (SQUIDs) and ultralow noise cryogenic HFET amplifiers reduce the thermal noise to below 100 mK [3]. This incredibly sensitive microwave receiver, extensive simulations and understanding of the apparatus allows the weak, quasi-monochromatic microwave signal resulting from an axion Primakoff interaction to be extracted from the noise [3].

B. ADMX G2 and Future Generations of ADMX

The current generation of ADMX has scanned a range of 500 to 850 GHz frequencies and will continue to scan up to 1 GHz. ADMX Generation 2 will use array of smaller cavities within same magnet locked to single frequency, and will scan 1 to 2 GHz. Above 2 GHz, experiments will require fine-tuning methods that satisfy space and noise constraints. A promising new tunable apparatus uses nonlinear dielectric films inside the microwave cavities. Changing the temperature and applying a voltage to the film changes the dielectric constant of the material: in turn, the resonant frequency of the cavity changes. This method provides three major advantages.

From Eq. 1, the variables η, $g_{a\gamma\gamma}$, ρ_a, m_a are dependent on axion theory. B_0 , V is the volume of the cavity, C, and Q_c, on the other hand, is dependent on the apparatus of the experiment.

1. The frequency of the cavity is $\propto \frac{1}{r_c}$, where r_c is the radius of the cavity. Therefore, coating the inside of the microwave cavity with a thin film with only have a very small impact on the volume of the cavity and it can retain a higher signal power. This is particularly crucial as the cavities become smaller to probe higher frequencies.

2. Nonlinear dielectric films like STO can change their behavior when biased and depending on the temperature. This tuning mechanism introduces very little additional thermal noise, which is important because the power signal is very weak.

3. Since $f \propto \frac{1}{\sqrt{\epsilon eff}} \propto E_\gamma \propto m_a$, a large shift in dielectric constant means that a large range of axion masses can be scanned.

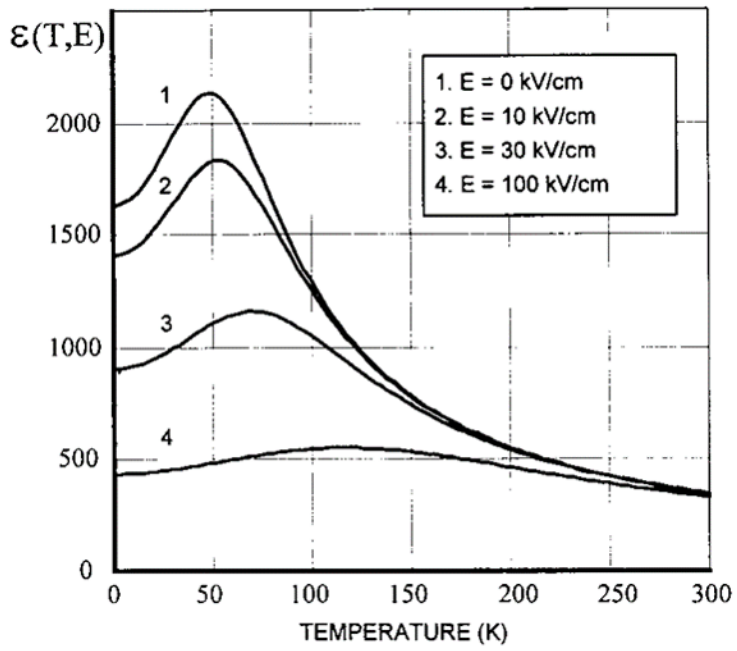

FIG. 3: Dependence of the dielectric constant of STO on Temperature [4]. Each curve is biased by fields of different magnitudes. In this experiment, no biasing fields were used, so the first curve is used as a reference.

Finally, in order for this technique to be used to tune the cavity accurately, the behavior of these nonlinear dielectric materials must be well understood.

III. NONLINEAR DIELECTRIC MATERIALS: STRONTIUM TITANATE

It is the goal of this project to characterize Strontium titanate (STO), a material with a nonlinear dielectric constant. At room temperature, it is a paraelectric material with a perovskite structure and dielectric constant of $\epsilon \approx 300$. At lower temperatures, $SrTiO_3$ displays ferroelectric properties and its dielectric constant increases to $\epsilon \approx 10^4$.

For this experiment, such a large shift in dielectric constant would cause too large a shift in resonant frequency. Collaborators at Virginia Tech used magnetron sputtering to deposit 1 and $5\mu m$ STO films on Quartz slides. The combination of Quartz with a dielectric constant of $\epsilon \approx 3.8$ and the thin layer of nonlinear dielectric material produces a noticeable but less extreme shift in resonant frequency. Ideally, the film should be as thin as possible to tune the desired frequency range and save space. The smoothness of the film and the evenness of deposition of the material on the cavity walls is also important to consider. Additionally, it may be cost-effective to combine STO with less expensive materials that potentially have better cohesion with the crystal structure of STO. The triagonal Quartz crystal structure match STO better than other materials such as Sapphire, minimizing the

unorganized interface between the two materials.Thus, in order to characterize STO, we must consider how the thickness and annealing of the STO films affect the resonant frequency, and how Quartz influences the behavior of the films.

IV. APPARATUS

The four samples of STO on quartz, the single pure quartz sample and the bare resonator were studied using a coplanar waveguide resonator, a cryostat, and a network analyzer. As mentioned in Section II B, the shift in frequency of the resonator is correlated to a shift in dielectric constant. This is the effective dielectric constant, ϵ_{eff}: the dielectric constant of STO must be isolated using other methods.

A. Coplanar Waveguide Resonator

The coplanar waveguide resonator used in this project with a sample is shown in Fig. 4, along with an HFSS model. It is made out of gold-plated copper and Rogers TMM10i

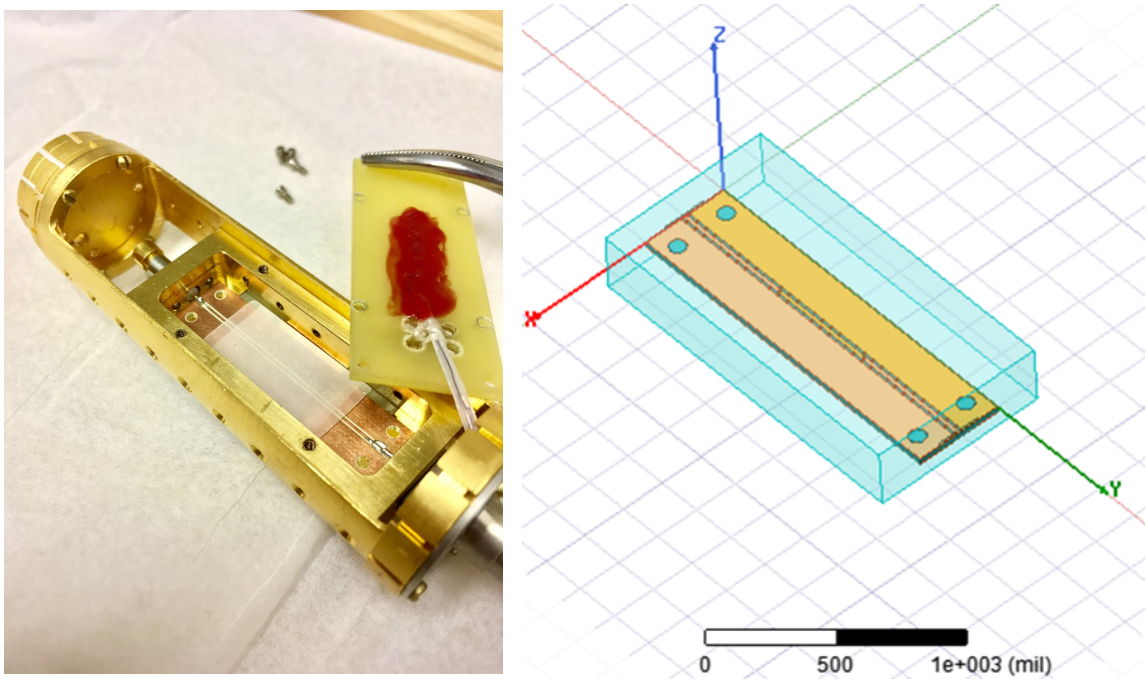

(a) CPWG Resonator with sample

(b) HFSS model of CPWG.

FIG. 4: The Coplanar Waveguide Resonator is mounted on a probe and is placed into the sample well of the cryostat.

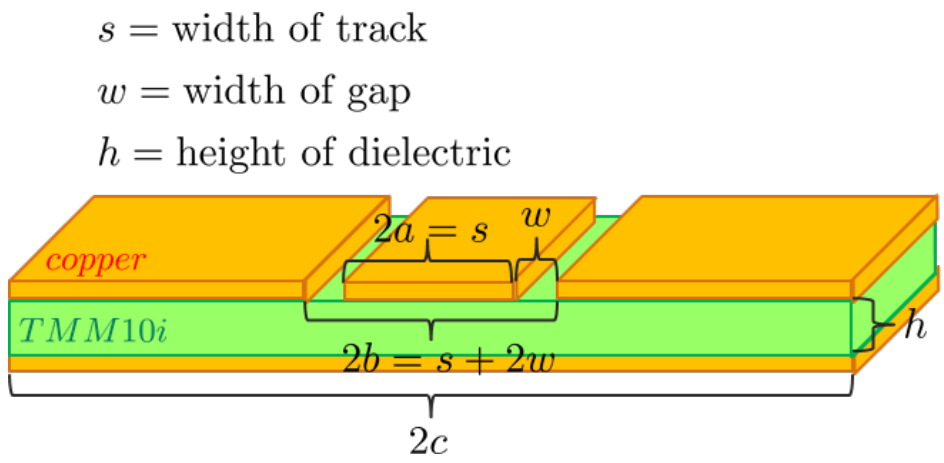

FIG. 5: Schematic of the Coplanar Waveguide Resonator.

substrate. In the center, there is an 8.99 mm half-wavelength resonator where the samples are centered. Two small pins attached to the lid of the resonator hold the sample firmly in place. This resonator is mounted on a probe that is put inside vertically inside the cryostat.

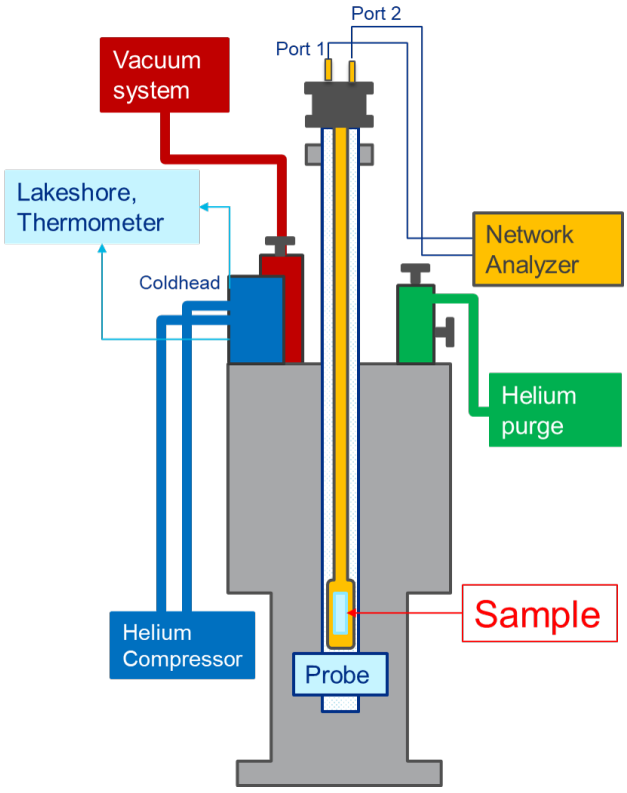

FIG. 6: Components of the Experiment.

B. Cryostat

The Cryostat, shown in Fig. 6, consists of a vacuum-insulated vessel with a sample well in the center. The resonator, along with the sample, is mounted on a probe and inserted into the vessel through the sample well. Helium is compressed and concentrated towards the bottom of the vessel, where it cools the resonator and sample. The temperature can be changed using the cryogenic temperature controller.

C. Obtaining the Frequency Spectra

The five samples are centered on the coplanar waveguide resonator, which changes the resonant frequency. The resonator with each sample is then put inside the cryostat, where it is monotonically cooled down to 6 K. The frequency response of the resonator is measured and recorded at different temperatures using the network analyzer. 16 frequency spectra were recorded for each sample from $T \approx 300$ to $T \approx 6$. For the STO on Quartz, the side without the STO film was measured as well. The dielectric constant as the temperature decreases can be extracted from the resonant frequencies in these spectra.

V. DATA

The resonant frequencies for all five samples and the bare resonator are shown in Fig. 7 and 8. Fig 7 shows the frequency spectra at several temperatures for the Bare Resonator, Quartz, and the STO on Quartz samples with the STO films in contact with the resonator. Fig. 8 shows all the STO on Quartz samples with the Quart sides on the resonator, with the STO films facing the lid.

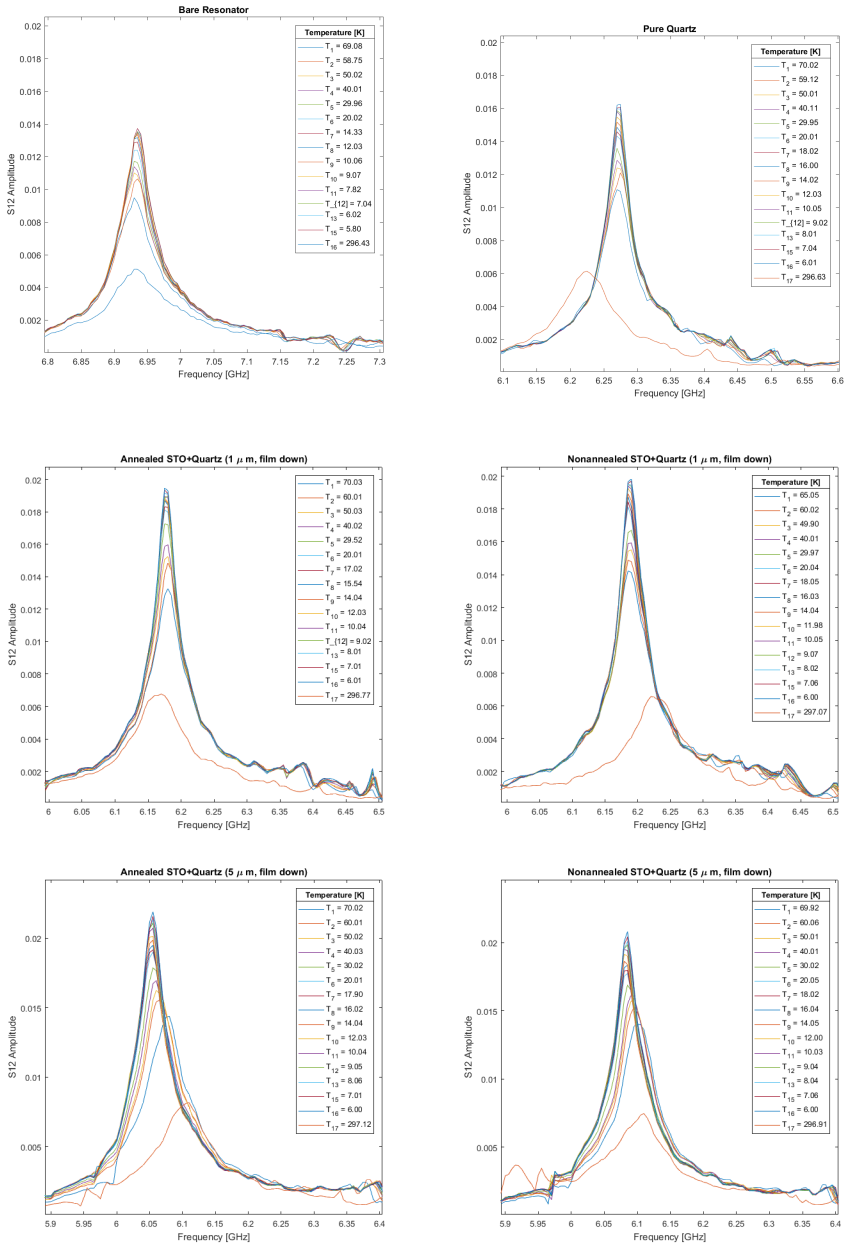

FIG. 7: Resonant peaks of each sample and temperatures at which they were taken.

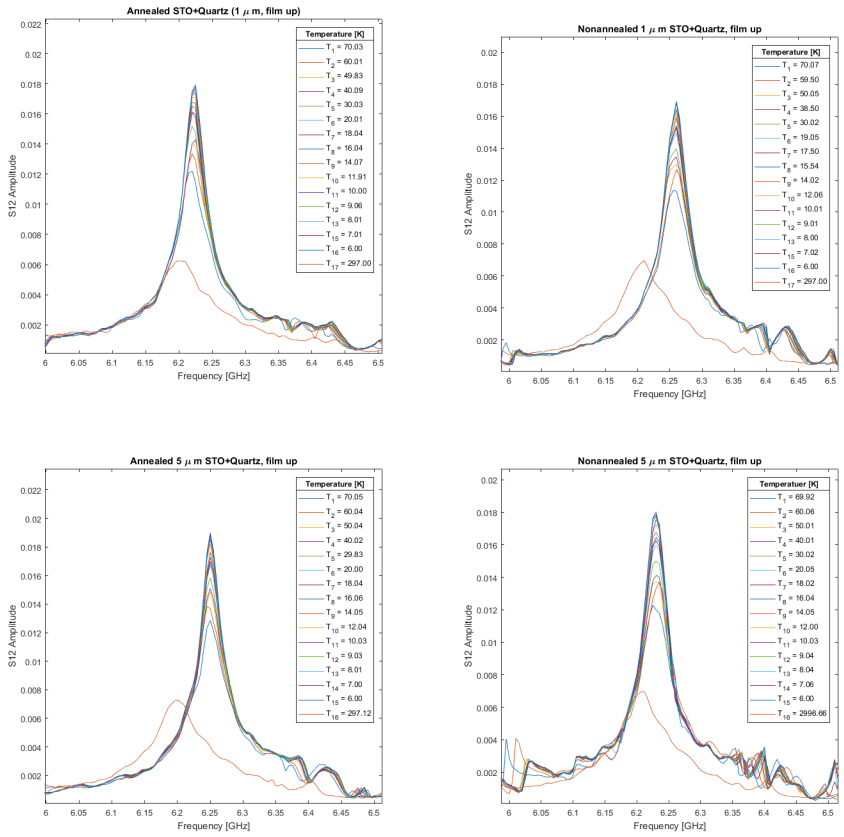

FIG. 8: The STO and Quartz samples are positioned in the resonator so that the unpolished Quartz side is on the resonator while the STO film faces the lid.

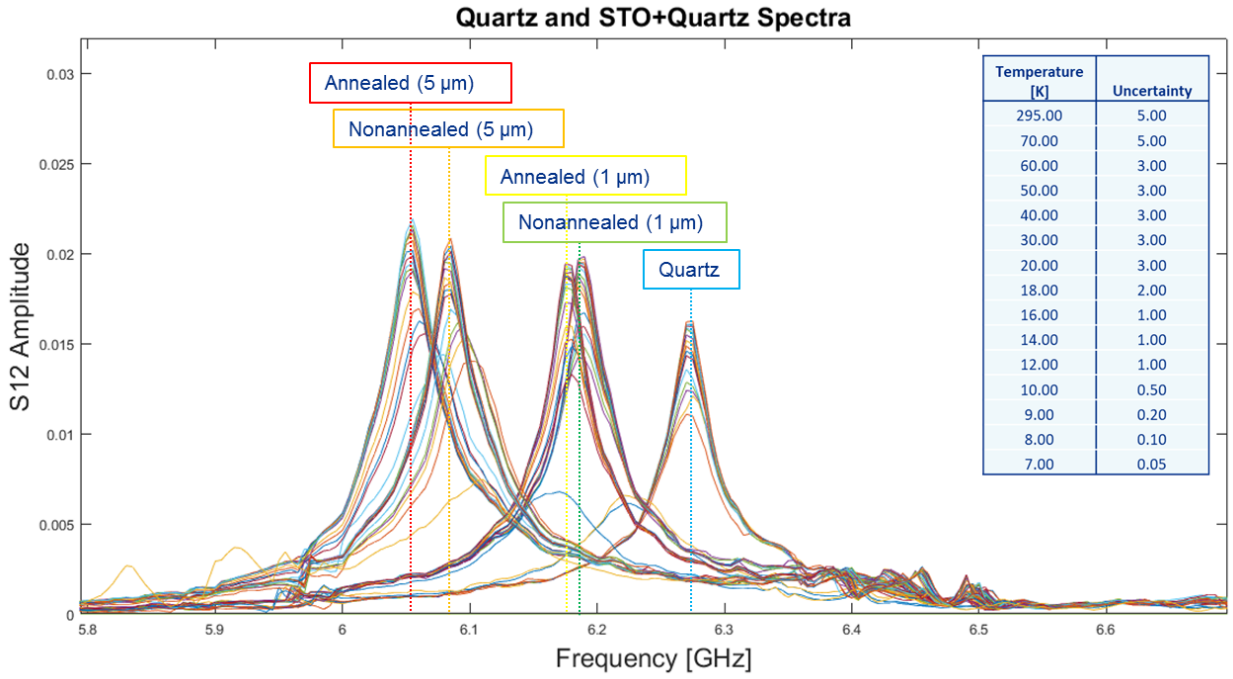

FIG. 9: Quartz and STO on Quartz samples.

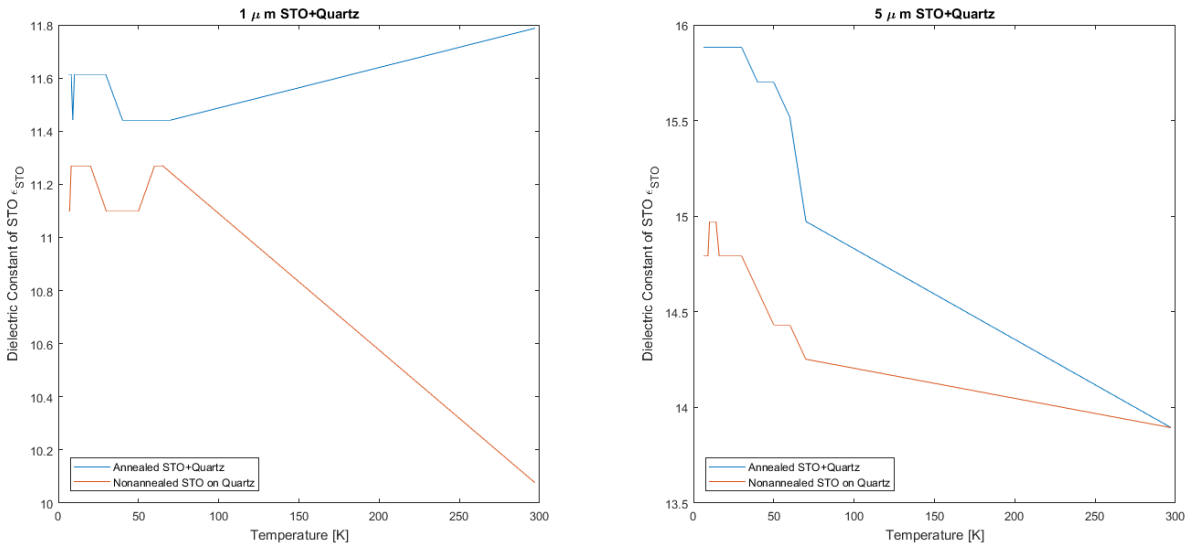

FIG. 10: Comparison of ϵ_{STO} vs. Temperature for the 1 μm and 5 μm annealed and nonannealed samples.

VI. RESULTS AND ANALYSIS

From Fig. **??**, the average resonant frequency of the bare resonator is $f_{av} = 6.9333$, the root mean square is 6.9333, and standard deviation is $s = 0.0024$. As the temperature

decreases, the resonant frequency and the dielectric constant remains fixed. Therefore, there is no significant contribution from thermal contraction to the shift in frequency. As shown in Fig. 9, the dielectric materials, Quartz and STO, are the cause of the shift in frequency and dielectric constant.

Then, the dielectric constant of STO can be extracted from this data. The effective dielectric constant for this half-wavelength resonator can be approximated by

$$\epsilon_{eff} = \left(\frac{c'}{f \times 2l}\right)^2 \tag{2}$$

where c' is the speed of light, l is the length of the resonator, and f is the resonant frequency. From the effective dielectric constant, the phase velocity can be directly calculated, and characteristic impedance is approximated from the geometry of the coplanar waveguide [5].

$$v_{ph} = \frac{c'}{\sqrt{\epsilon_{eff}}} \tag{3}$$

$$Z_0 = \frac{60\pi}{\sqrt{\epsilon_{eff}}} \frac{K(k_0')}{K(k_0)} \tag{4}$$

$$\text{where} \quad k_0 = \frac{c}{b}\sqrt{\frac{b^2 - a^2}{c^2 - a^2}} \quad \text{and} \quad k_0' = \sqrt{1 - k_0^2} \tag{5}$$

Here, K(k), is the elliptic integral, and a, b and c are defined in Fig. 5 and 11. This allows us to calculate the total capacitance of the coplanar waveguide, since

$$C_{total} = \frac{1}{Z_0 v_{ph}} \tag{6}$$

Another way to obtain ϵ_{eff} is by using the equation

$$\epsilon_{eff} = \frac{C_{total}}{C_0} \tag{7}$$

$$C_0 = 4\epsilon_0 \frac{K(k_0')}{K(k_0)} \tag{8}$$

where C_0 is also the capacitance of the line by itself. Letting the E-field exist in one dielectric layer at a time [6], the coplanar waveguide resonator has two dielectric layers above it, STO and Quartz, and one vacuum or air layer above those two. The capacitance

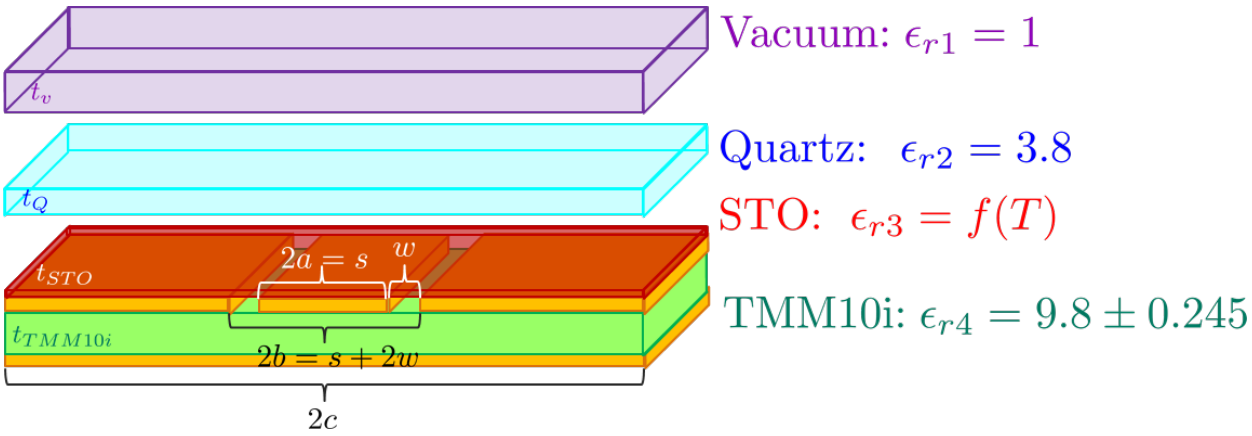

FIG. 11: Layers of Dielectric Material on the Coplanar Waveguide Resonator.

at each layer is approximated by [6]:

$$C_0 = 4\epsilon_0 \frac{K(k_0')}{K(k_0)} \tag{9}$$

$$C_1 = 2\epsilon_0 \epsilon_{r1} \frac{K(k_1')}{K(k_1)} \tag{10}$$

$$C_2 = 2\epsilon_0 (\epsilon_{r2} - \epsilon_{r1}) \frac{K(k_2')}{K(k_2)} \tag{11}$$

$$\boxed{C_3 = 2\epsilon_0 (\epsilon_{r3} - \epsilon_{r2}) \frac{K(k_3')}{K(k_3)}} \tag{12}$$

$$C_4 = 2\epsilon_0 (\epsilon_{r4} - 1) \frac{K(k_4')}{K(k_4)} \tag{13}$$

where: (14)

$$k_0 = \frac{c}{b}\sqrt{\frac{b^2 - a^2}{c^2 - a^2}} \qquad k_0' = \sqrt{1 - k_0^2} \tag{15}$$

$$k_i = \frac{\sinh(\frac{\pi c}{2h_i})}{\sinh(\frac{\pi b}{2h_i})}\sqrt{\frac{\sinh^2(\frac{\pi c}{2h_i}) - \sinh^2(\frac{\pi a}{2h_i})}{\sinh^2(\frac{\pi c}{2h_i}) - \sinh^2(\frac{\pi a}{2h_i})}} \qquad k_i' = \sqrt{1 - k_i^2} \tag{16}$$

where,

$$h_1 = t_v + t_Q + t_{STO} \tag{17}$$

$$h_2 = t_Q + t_{STO} \tag{18}$$

$$h_3 = t_{STO} \tag{19}$$

$$h_4 = t_{TMM10i} \tag{20}$$

are defined by Fig. 5. Now, since $C_3 = C_{total} - (C_1 + C_2 + C_4)$ is the capacitance of the STO layer, the dielectric constant is isolated into

$$\epsilon_{STO} = \frac{C_{STO}}{2\epsilon_0} \frac{K(k_{STO})}{K(k'_{STO})} + \epsilon_{Quartz} \tag{21}$$

where C_{total} is from Eq. 6, ϵ_{Quartz} is given as 3.8 and the elliptical integrals rely on the geometry of the resonator. A similar calculation was done for the pure quartz layer, with an error of 6.17%. Figure 10 shows ϵ_{STO} calculated using this method vs. Temperature. The curve of the thicker STO samples at low temperatures resemble curve 1 in Fig. II B. The thinner STO samples do not behave as expected. Observing the pure quartz sample and the samples in which the unpolished quartz side is in contact with the resonator, it appears that the dielectric constant of quartz also varies considerably with temperature. It decrease as the temperature decreases and this effect overwhelms the large dielectric shift that STO is expected to undergo at lower temperatures.

This effect is difficult to take into consideration in an analytic model unless the variability of ϵ_{Quartz} is also taken into consideration.

VII. CONCLUSION

The frequency response of coplanar waveguide resonator with the annealed and nonannealed STO on Quartz samples is due to the dielectric properties of the films and not due to thermal contraction. Frequencies shift downward for the STO+Quartz samples, indicating that the dielectric constant is increasing with decreasing temperature. The thickness of the sample is the parameter with the greatest impact on the frequency and dielectric constant, partly because the ϵ_{Quartz} decreases, negating the expected increasing ϵ_{STO}. Whether the

sample is annealed or not is a secondary attribute that has a minor effect on the frequency shift and peak width. The dielectric constant vs. temperature curve promisingly displays similar behavior to that observed by Vendik, et al. in Figure II B, and a similar model based on pure quartz and crosschecked gives an error of 6.17%. However, the frequency shifts and the corresponding dielectric changes are not of the expected magnitude, and are not detailed enough to conclude that the STO films are approaching a ferroelectric transition. We conclude that while it is valuable to use STO films for their tunability, more research with pure STO samples is required. Future work includes building a resonator that can be voltage biased, obtaining a more detailed sampling of resonant frequencies and developing a more accurate analytic model of the coplanar waveguide resonator that can take the changing dielectric constant of Quartz into account.

[1] Adms: Axion dark matter experiment. `http://depts.washington.edu/admx/index.shtml`. Accessed: 08-15-2017.

[2] J.V. Sloan, M. Hotz, C. Boutan, R. Bradley, G. Carosi, D. Carter, J. Clarke, N. Crisosto, E.J. Daw, J. Gleason, J. Hoskins, R. Khatiwada, D. Lyapustin, A. Malagon, S. OKelley, R.S. Ottens, L.J. Rosenberg, G. Rybka, I. Stern, N.S. Sullivan, D.B. Tanner, K. van Bibber, A. Wagner, and D. Will. Limits on axionphoton coupling or on local axion density: Dependence on models of the milky ways dark halo. *Physics of the Dark Universe*, 14:95 – 102, 2016.

[3] S. K. Lamoreaux, K. A. van Bibber, K. W. Lehnert, and G. Carosi. Analysis of single-photon and linear amplifier detectors for microwave cavity dark matter axion searches. *Phys. Rev. D*, 88:035020, Aug 2013.

[4] O. G. Vendik, E. K. Hollmann, A. B. Kozyrev, and A. M. Prudan. Ferroelectric tuning of planar and bulk microwave devices. *Journal of Superconductivity*, 12(2):325–338, Apr 1999.

[5] Brian C. Wadell. *Transmission Line Design Handbook*. Artech House, 4th edition, 1991.

[6] R. N. Simons. *Coplanar Waveguide with Finite-Width Ground Planes, in Coplanar Waveguide Circuits, Components, and Systems*. John Wiley and Sons, Inc., 2001.

[7] Leslie J. Rosenberg. Dark-matter QCD-axion searches. *Proceedings of the National Academy of Sciences*, 112(40):12278–12281, October 2015.

[8] Stephen J. Asztalos, Leslie J Rosenberg, Karl van Bibber, Pierre Sikivie, and Konstantin Zioutas. Searches for astrophysical and cosmological axions. *Annual Review of Nuclear and Particle Science*, 56(1):293–326, 2006.

[9] Daniel Bowring. Advanced computing for next-generation dark matter searches. Applied and computational mathematics seminar, UW-Madison, 2017.

[10] Davide Cadamuro. Cosmological limits on axions and axion-like particles, October 2012.